water

MDPI

Article

Forecasting the Failure Time of an Expansive Soil Slope Using Digital Image Correlation under Rainfall Infiltration Conditions

Xueyun Wei [1,2,3,4], Wenwei Gao [5,*], Ruilin Hu [1,2,3], Wei Gao [6], Yidi Qiu [7] and Yong Li [7]

1 Key Laboratory of Shale Gas and Geo-Engineering, Institute of Geology and Geophysics, Chinese Academy of Sciences, Beijing 100029, China; wei_xueyun@163.com (X.W.)
2 Institutions of Earth Science, Chinese Academy of Sciences, Beijing 100029, China
3 College of Earth and Planetary Sciences, University of Chinese Academy of Sciences, Beijing 100049, China
4 College of Architecture Engineering, Quzhou University, Quzhou 324000, China
5 Department of Architecture and Engineering, Yan'an University, Yan'an 716000, China
6 Department Active Structure Exploration, China Earthquake Disaster Prevention Center, China Earthquake Administration, Beijing 100029, China
7 College of Geosciences and Surveying Engineering, China University of Mining and Technology, Beijing 100083, China
* Correspondence: gaowenwei@yau.edu.cn

Highlights:

What are the main findings?

- Digital image correlation (DIC) method was applied to monitor the slope surface deformation and crack development.
- Deformation and failure processes of the expansive soil slope had an obvious crack control effect.
- The SLO method should be preferentially used to forecast the failure of expansive soil slopes with "step-like" displacement.

What is the implication of the main findings?

- The main findings are helpful for forecasting expansive soil landslides and providing guidance for controlling landslide hazards in expansive soil areas.

Abstract: Expansive soil is one of the most widely distributed special soils in the world. It is widely developed in Henan, Anhui, Guangxi and other places in China, and highly overlaps with densely populated and economically active areas. Expansive soil is considered a typical "problematic soil" because its mechanical behaviour is very sensitive to water content changes; such behaviour mainly manifests as swelling upon wetting and shrinking upon drying, so the presence of expansive soil is an important factor in mountain landslide disasters in southern China. Because the particularities of its constituent materials are related to typical physical and mechanical properties, forecasting the failure times of expansive soil slopes remains a global problem. In this study, a series of in situ artificial rainfall experiments were conducted on an excavated expansive soil slope; then, the digital image correlation (DIC) method was applied to monitor the slope surface deformation and crack development. Finally, the failure time of the slope was forecasted using the inverse velocity (INV) and slope (SLO) models. The study results show that the deformation and failure processes of the analysed expansive soil slope had an obvious crack control effect, and the displacement–time curve derived by the DIC method had an obvious "phased change law". The data points calculated by the INV method were discrete and had high linear fitting requirements, resulting in large failure time forecasts. When the SLO method was used to forecast the failure time, because the values derived in the stable deformation stage were relatively concentrated in the calculation process, an obvious linear relationship was found in only the accelerated deformation stage, so the prediction results were more accurate. Therefore, the SLO method should be preferentially used to forecast the failure

check for updates

Citation: Wei, X.; Gao, W.; Hu, R.; Gao, W.; Qiu, Y.; Li, Y. Forecasting the Failure Time of an Expansive Soil Slope Using Digital Image Correlation under Rainfall Infiltration Conditions. *Water* **2023**, *15*, 1328. https://doi.org/10.3390/w15071328

Academic Editor: Echuan Yan

Received: 9 March 2023
Revised: 22 March 2023
Accepted: 25 March 2023
Published: 28 March 2023

of expansive soil slopes with "step-like" displacement. These results enabled us to characterize slide processes and identify the mechanism responsible for the movement of a rainfall-induced expansive soil landslide. The stage deformation and failure mode of expansive soil landslide under rainfall infiltration: "slow deformation—stable deformation—accelerated deformation—instability failure" was revealed. This study is helpful for determining the deformation and failure mechanism of rainfall-induced expansive soil landslide and forecasting expansive soil landslides and providing guidance for controlling landslide hazards in expansive soil areas.

Keywords: expansive soil; field test; digital image correlation (DIC); landslide forecast; prediction model

1. Introduction

Expansive soil, a common soil type, is widely distributed across the world except in the Arctic region [1,2]. Because expansive soil contains many clay minerals, such as montmorillonite and illite, it has strong hydrophilicity, water absorption-expansion, softening, disintegration, water loss-shrinkage, cracking, and hardening tendencies and is extremely unstable, thus introducing potential safety hazards to engineering construction. Expansive soil is also a "problematic soil" that has plagued geotechnical workers for many years [3]. In the field of geotechnical engineering, the remediation of expansive soil and the landslide caused by it do great harm to the people and the country.

The engineering problems caused by expansive soil are related to its three typical physical and mechanical properties: expansion and contraction, cracking, and overconsolidation [4]. To date, extensive research has explored the characteristics of expansive soil, and important progress has been made [5–8]. Due to the particular physical mechanics of expansive soil itself and its sensitivities to changes in climate, rainfall and other external environmental factors, the instability of expansive soil slopes has been difficult to ponder [9,10]. Scholars have analysed the instability mechanisms of expansive soil slopes through different methods. The topics of published research can be summarized as follows: the influence of the expansive soil strength on slope stability [11,12], the effects of the fissure and permeability characteristics of expansive soil on slope stability [13–16], the failure characteristics of expansive soil slopes under freeze–thaw cycles [17,18], the scouring and stability characteristics of expansive soil slopes with different dip angles [19], and the coupling of factors influencing expansive soil slopes, such as the slope steepness and vegetation [20]; the conclusions obtained in the above research on expansive soil slopes have been of great help in achieving the reinforcement of expansive soil slopes [21,22].

The key to scientifically reducing disasters caused by expansive soil landslides is to accurately forecast imminent landslide precursors to realize their prediction and early warning. Generally, the permeability coefficients of expansive soils measured based on indoor tests are very small, so it is theoretically difficult for rainwater to infiltrate these soils [4]. Existing studies have also shown that the instability of expansive soil slopes is generally dominated by shallow sliding in rainy weather [23]. It is found that the instability of expansive soil slope is at its peak during or just after the rainy season. This is because the alternate change of dry and wet climate causes the expansion and contraction of expansive soil. While the primary fissure is further expanded, a large number of secondary fissures are further generated. The development of fissure undoubtedly opens the preferential channel for rainwater intrusion and water evaporation, and rainfall infiltration leads to the change of soil properties. Surface deformation is the most intuitive landslide response observed before slope stability is reduced, and instability failure occurs under the combined action of various factors. Therefore, monitoring methods based on landslide deformation data are the most effective [24]. Predictive research regarding slope deformation and failure times began in the 1960s and mainly involves the use of empirical formulas to predict failure times from the relationship between the logarithm of the creep failure

time and the strain rate in the secondary creep stage [25]. The inverse velocity (INV) model was based on the reciprocal of the relationship between the slope displacement rate and time [26], while the slope (SLO) model was designed to predict the displacement velocity of slopes [27]; a landslide displacement prediction method was designed based on time series and the genetic algorithm-support vector regression (GA-SVR) coupling model [28]. Considering the influence of the soil structure and the occurrence of fractures in expansive soil, in situ displacement observations are the most direct and persuasive theoretical method for studying expansive soil. The digital image correlation (DIC) method, an optical measurement method proposed in the 1980s [29], is widely used to monitor slope deformation because of its simple operation, noncontact nature, capacity to obtain full-field measurements, real-time characteristics and other advantages [30–32]. Therefore, DIC is an extremely effective means for monitoring the deformation of expansive soil slopes.

Due to the expansion-contraction and fissure properties of expansive soil, coupled with the compound superposition of external environmental effects, especially the very complex geometry structure of the fracture network in expansive soil, and the uncertain formation and development process, it is unable to form an effective early warning method of expansive soil landslide disaster at the present stage. Therefore, on the basis of grasping the disaster mechanism of expansive soil landslide, it is of great significance to carry out the research on early identification and warning of landslide disaster.

To more accurately understand the development of instability and failure in expansive soil slopes under rainfall infiltration, a series of in situ artificial rainfall experiments were conducted on an excavated expansive soil slope in Pishihang, Anhui Province, China. The DIC method was applied to monitor the slope surface deformation and crack development processes. The results enabled us to characterize the slide processes and identify the mechanism responsible for the movements of rainfall-induced expansive soil landslides. The systematic study will enrich and reveal the failure mode and disaster mechanism of crack slope. The results of this study will be helpful for predicting expansive soil landslides and providing guidance for controlling landslide hazards in expansive soil areas.

2. Method

2.1. DIC Method

DIC is a new noncontact optical method for obtaining full-field displacement and deformation measurements [33]. Figure 1 shows the field schematic diagram derived using the DIC method with slope deformation measurements. The main processes were as follows: (1) the monitoring points were set according to the landslide scale, and each point was equipped with a camera and other image acquisition equipment. The image acquisition equipment was selected while comprehensively considering the complex climatic conditions at the survey site, the observation distance and the observation angle. (2) The slope was continuously photographed by the image-acquisition equipment to obtain time series images. (3) These images were analysed by digital image processing methods to obtain motion quantities, such as the position, velocity and acceleration, and shape variables, such as displacement and strain [34].

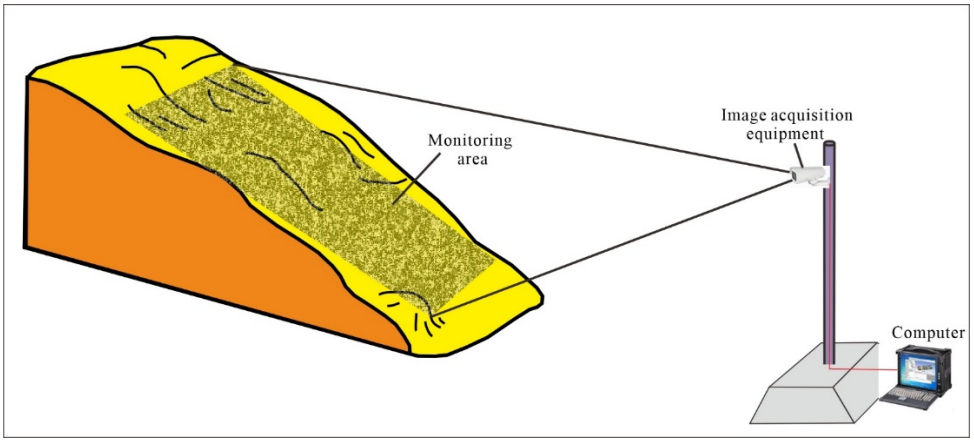

Figure 1. Field diagram of slope deformation measurements derived with the DIC method.

2.2. Landslide Forecast Model Based on Surface Displacement

2.2.1. INV Model

In indoor tests, Ref. [35] induced failure on various sandy slopes by simulating rainfall. Three types of inverse-velocity plots fitted to laboratory data were presented, finally concluding that a linear fit through the inverse-velocity against time data provided a reasonable estimate of failure-time, shortly before failure [27]. Through integrations and formula transformations, the following expression was obtained:

$$\frac{1}{v} = [a(\alpha - 1)]^{\frac{1}{\alpha - 1}} (t_r - t)^{\frac{1}{\alpha - 1}} \quad (1)$$

where $\frac{1}{v}$ is the reciprocal of the deformation rate, t is time, t_r is the failure time, and a and α are constants. Therefore, the INV method was proposed. When $\alpha = 2$, the $1/v$-t relationship curve is linear; when $1 < \alpha < 2$, the curve is concave; and when $\alpha > 2$, the curve is convex. Tests showed that when α varies in the range of 1.5~2.2, the typical model shown in Figure 2 is obtained [24]. When $\alpha = 2$, the intersection of the straight line and the time axis is the forecasted failure time; when $\alpha \neq 2$, the tangent line at any time point or the method provided by [35] can be used to roughly predict the failure time. Because of the simplicity of the linear curve, α is generally assumed to be 2 in actual slope failure predictions.

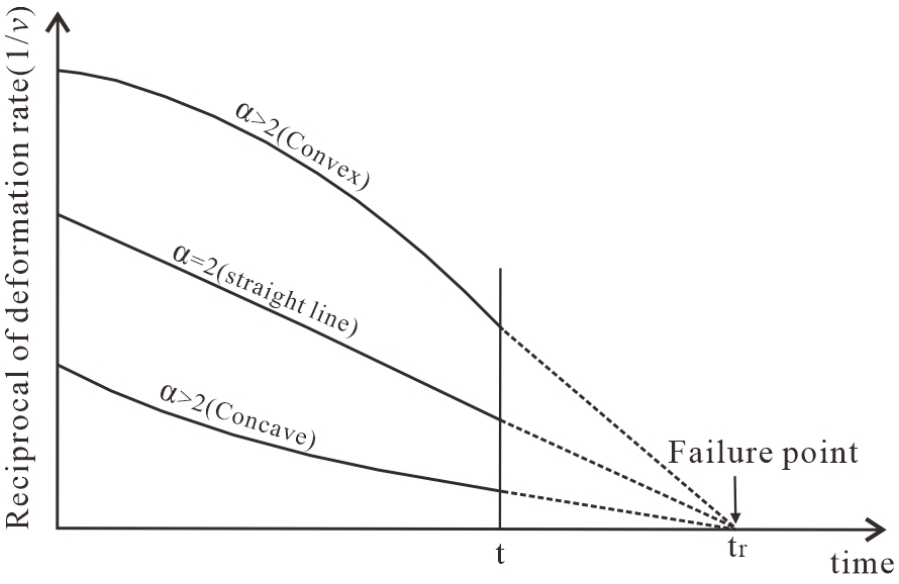

Figure 2. Plot of the INV model [35].

2.2.2. SLO Model

Based on Formula (1) and assuming $\alpha = 2$, Ref. [27] proposed the following SLO model:

$$\frac{du}{dt} = \frac{B}{t_r - t} \tag{2}$$

where $\frac{du}{dt}$ is the deformation rate, t is the time, t_r is the failure time, and B is a constant. Formula (2) can be rearranged to obtain the following expression:

$$t\frac{du}{dt} = t_r\frac{du}{dt} - B \tag{3}$$

where the slope of the relationship curve $t\frac{du}{dt} - \frac{du}{dt}$ is the forecasted failure time.

2.3. Overview of the Study Area

The study area was located on the riverside slope of the Wadong main canal in Pishihang Irrigation District, Hefei city, Anhui Province, at coordinates of 32°3′50″ N latitude and 116°54′21″ E longitude and 40 m above sea level. This location belongs to Yanliu town, Shouxian County, as shown in Figure 3a, and is situated in the northern Jianghuai watershed, a hilly area with undulating topography. The general terrain trend in this town is high in the southeast and low in the northwest. The study area has a subtropical semimonsoon humid climate with four distinct seasons, moderate rainfall, sufficient sunshine and mild climate conditions. The dominant wind directions throughout the year are east and northeast, the annual average temperature is 15.4 °C, and the annual average sunshine duration is 2523 h, accounting for 51% of the annual sunshine hours. The annual average rainfall is 903.2 mm, the annual maximum rainfall is 1534.1 mm and the daily maximum rainfall is 109 mm. In the study area, rainfall is mainly concentrated from May to September, the flood season.

The soil on the studied slope is mainly yellowish-brown expansive soil, with miscellaneous fill at the top. It belongs to the Quaternary overburden area, the Upper Pleistocene alluvial and diluvial (Q3al-pl) clays. The composition of soil particles is mainly fine powder with the content of 58.44~65.66%, clay content of 33.89~41.13%, and colloid content of 19.18~24.87%, natural water content of 22.1~28.3%, and natural density of 1.9–2.05 g/cm^3. The free expansion rate is 35~60%, belonging to the medium and weak expansive soil. Landslides have occurred in this area, with an average thickness of 4 m and a sliding volume of 14,000 m^3. These landslides have intruded into the river channel, as shown in Figure 3b,c. At present, the study site has reached a stable state.

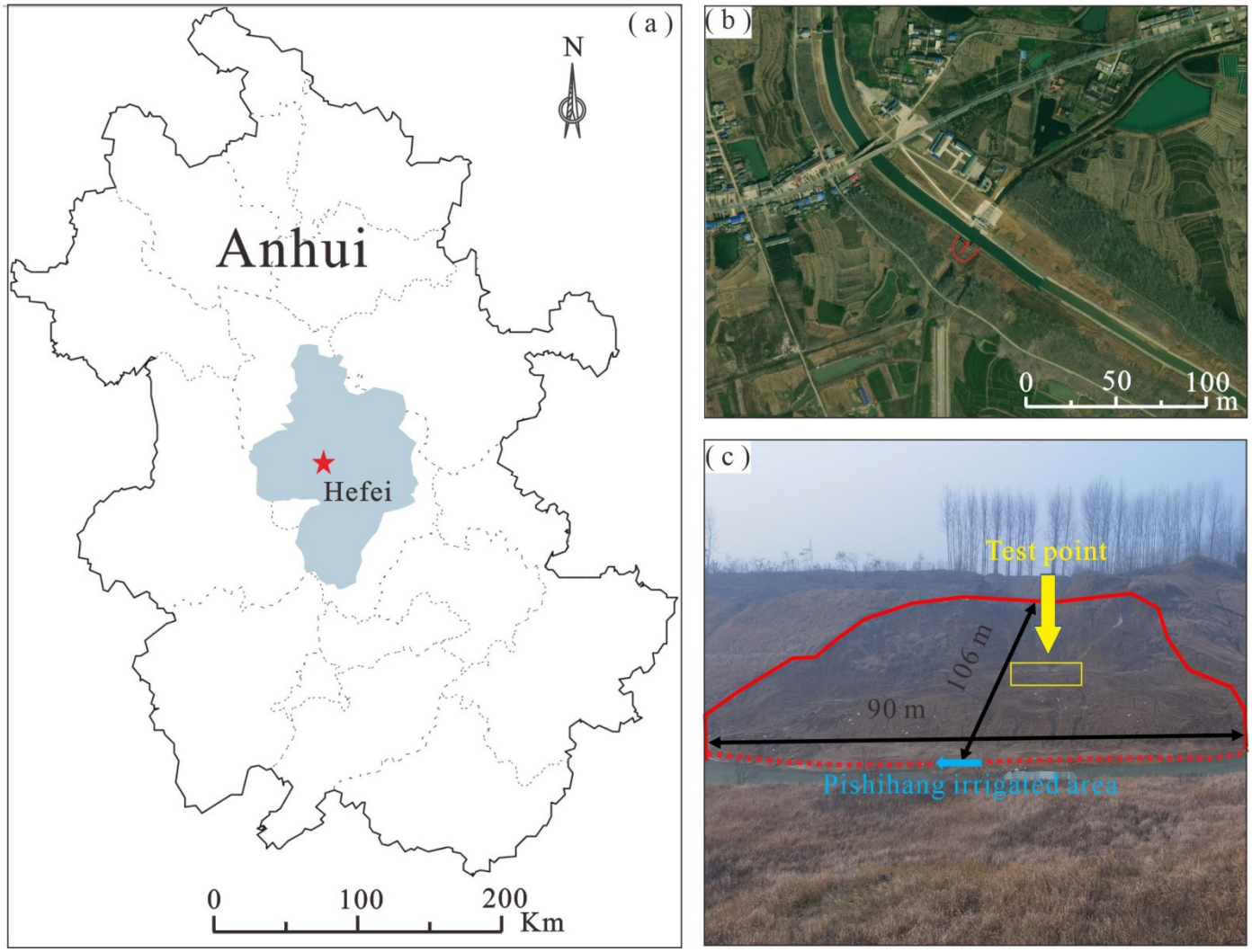

Figure 3. Location and geological map of the study area: (**a**) location of the study area; (**b**) satellite image of the slope (the base map was produced courtesy of Google Earth); and (**c**) overall view of the slope.

2.4. Testing Equipment

Since the sample site is located on the landslide mass, to eliminate the disturbance impact of landslides and surface human activities on the soil mass, the test machines and tools were excavated downwards to the disturbed expansive soil boundary, as shown in Figure 4a, and then an artificial slope with a planar area of 2 m × 1 m and a height of 2 m was excavated. The slope size is shown in Figure 4b. The excavated slope was approximately vertical due to site condition limitations, which conveniently allowed the camera to take crack images. To reasonably set the camera position and accurately set the data acquisition time interval, a calibration slope (Figure 4b: test slope No. 0) of the same size was excavated on the left side of the main test slope (Figure 4b: test slope No. 1) for pretest simulations and to calibrate the data acquisition system.

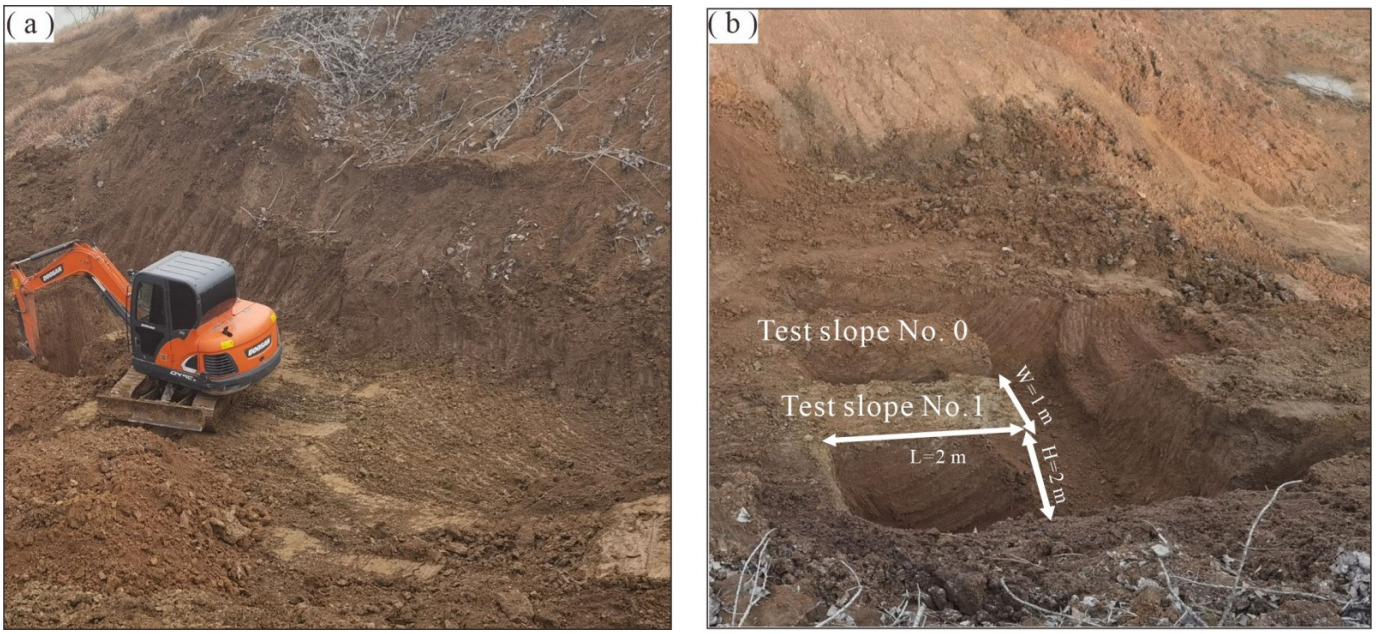

Figure 4. Test site preparation: (**a**) soil excavation; and (**b**) slope layout and size information.

The pre-experiment was carried out on the calibration slope under constant rainfall conditions to obtain the optimal camera shooting position and angle; see Figure 5a for these specific parameters. According to the low-permeability characteristics of expansive soil, to prevent surface rainwater from scouring the slope and ensure the rainfall infiltration effect, a two-layer water immersion tank with a height of 10 cm was built at the top of the test pit, as shown in Figure 6b. Referring to the rainfall intensity classification of the China Meteorological Administration and considering the influence of evaporation, the design adopted the single-dry-wet-cycle mode of artificial rainfall during the day and natural drying at night; to facilitate this, a precipitation nozzle was arranged on the top of the slope to simulate light to moderate rainfall conditions. The 24-h rainfall value was set to 11 mm, and wetting was performed until the slope was completely unstable and damaged.

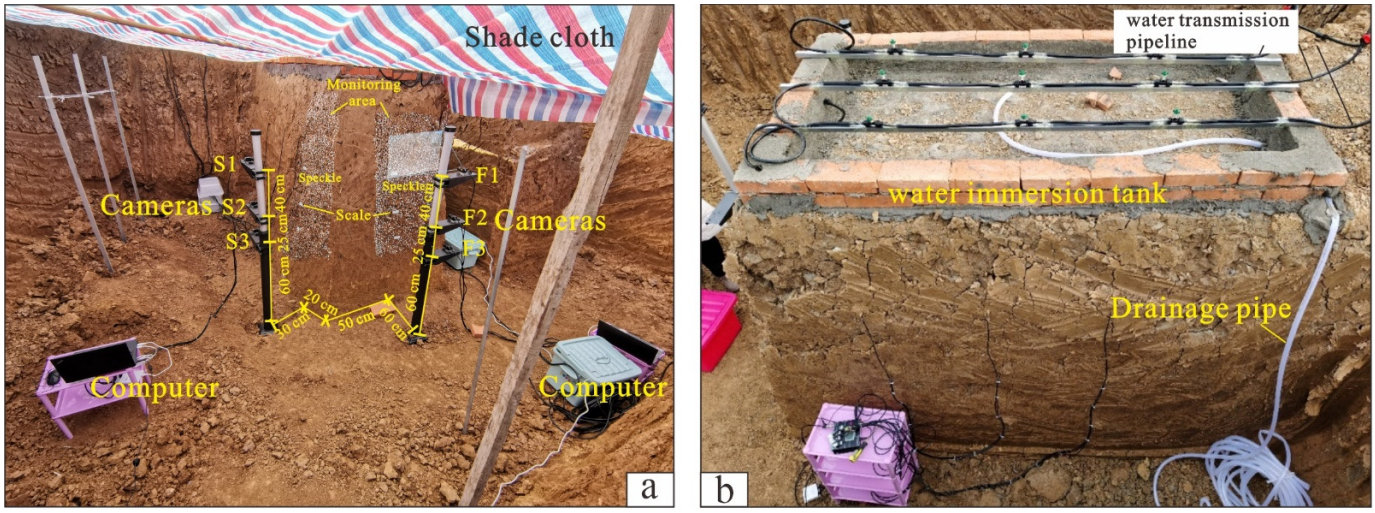

Figure 5. *Cont.*

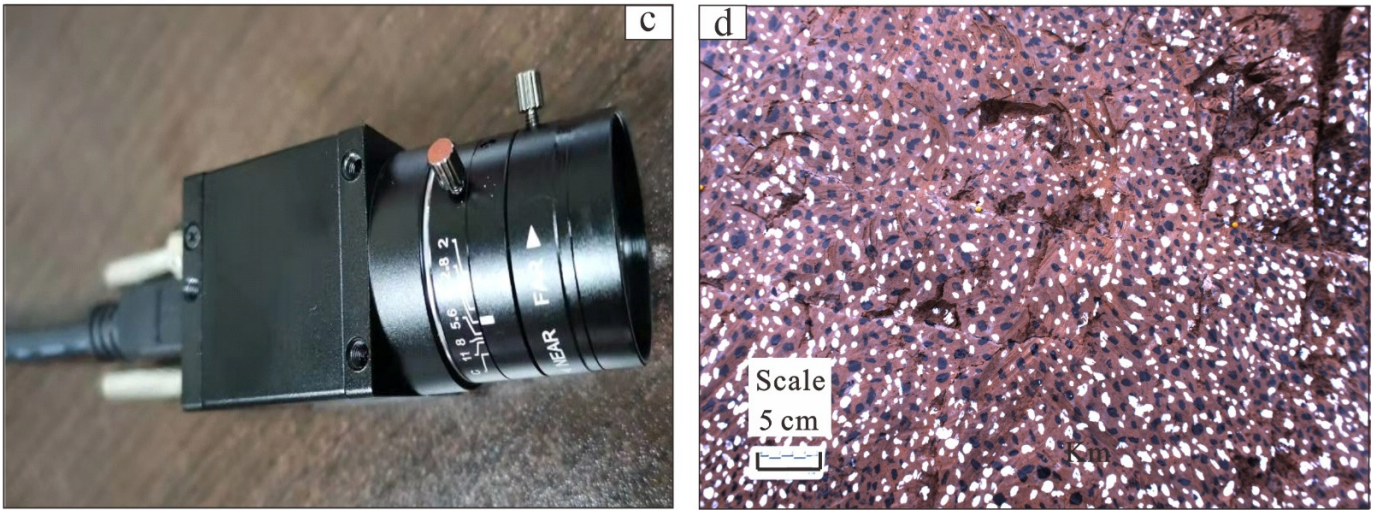

Figure 5. The layout of the test showing (**a**) the establishment of the experimental system; (**b**) the artificial rainfall simulator; (**c**) the image acquisition equipment; and (**d**) the image acquisition results (captured by camera F1 in (**a**)).

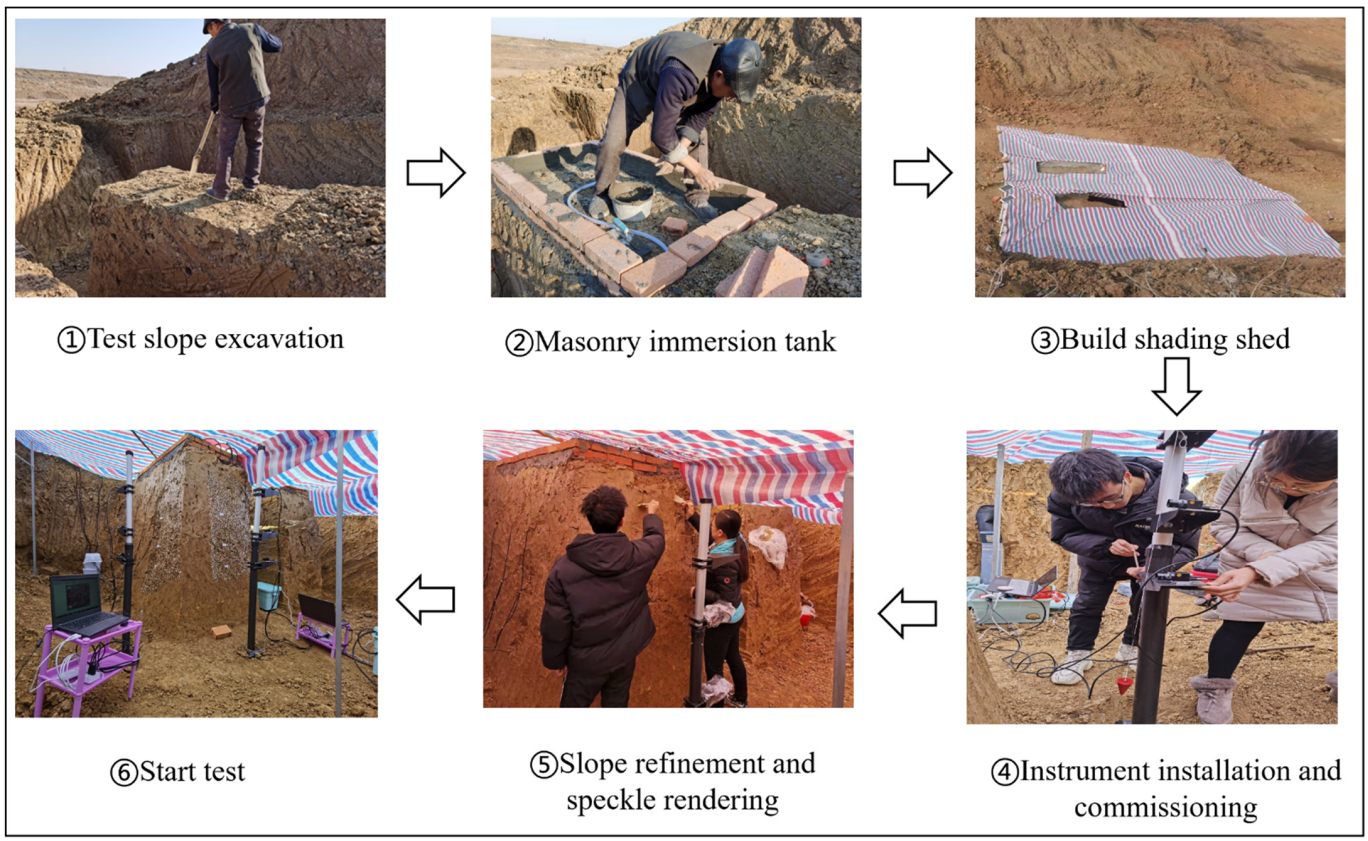

Figure 6. The main steps of the performed tests.

The displacement monitoring of the DIC method is based on digital photographs taken at different monitoring time points. Therefore, it can obtain the displacement of only two-dimensional images in each image sequence, and due to the limitations of the camera resolution and image acquisition range, it is impossible to obtain the three-dimensional deformation inside the slope in this test. To ensure that the obtained image can include the areas of possible deformation of the slope as much as possible, three industrial cameras with different heights were arranged at the front and side of the slope (Figure 5a). Huateng

Weishi model HT-SUA1600C-T cameras with resolutions of 16 million pixels were used (Figure 5c). The size of each speckle image was 52 cm × 40 cm (Figure 5d); cameras F1, F2 and F3 shot the front of the slope from top to bottom, and cameras S1, S2 and S3 shot the sides of the slope from top to bottom. During the test, the lens of each fixed camera was set parallel to the slope surface to ensure that the captured image reflected the real displacement characteristics.

2.5. Test Scheme and Process

The specific test process was divided into the following steps, as shown in Figure 6. (1) In the test slope excavation, according to the survey data, the site was excavated to the fissured grey–white expansive soil layer below the surface, the site was levelled and measured, and the specific location of the test slope was marked. The slope had an excavation depth of 2 m, a width of 1 m and a height of 2 m. (2) Regarding the masonry of the water immersion tank, the top of the test pit was levelled, and a 2 m × 1 m area was built at the top of the test pit with two layers of brick walls with a height of 10 cm. A drainage pipe was arranged at the rear of the left side of the test pit. (3) A shading shed was built; a support frame was set up around the test slope, and a shed cloth was used to block the natural light source, in order to reduce the impact of the light difference on the picture image and avoid the soil to dry. Two 40-W stable light sources were set up in the shed to reduce the impact of the light difference. (4) The instrument was installed and commissioned by setting up an industrial camera, adjusting the positions of the camera and the column, correcting the verticality of the cross-arm of the column with a heavy hammer, and assembling and commissioning the camera to ensure that it could record normally without Wi-Fi capabilities and after undergoing power failures and reconnections (to ensure 24-h uninterrupted photography). After commissioning, the camera was treated with moisture and antifreeze. (5) The slope refinement and speckle rendering processes were completed, and the scale was set. (6) The test was started: the slope was allowed to stand still for a given period until all data collectors were functioning stably; then, artificial rainfall commenced according to the specified rainfall scheme.

According to the test results obtained on the calibration slope, from the start of the test, the image acquisition interval was set to 60 min. When the slope began to undergo strong instability and failure (at approximately 3030 min), the shooting interval was shortened to 10 min; soil surface images were taken over the whole duration of the test.

3. Results

The change in the position of the speckles on the slope surface can be used to calculate the displacement. The DIC method is a mature method; traditionally, the first image is called the reference image (undeformed image), and the loaded image is called the deformed image. DIC matches the same pixels on the reference image and the deformed image, compares these pixels, and calculates the local horizontal and vertical displacement magnitudes of these points in the X and Y directions by comparing the two images [33]. To eliminate the error caused by distortion during photography, the camera was calibrated with a calibration plate before the test is carried out, the circular spacing of the plates was determined from the figure, and the relationship between the image pixels and real distance was established [36]. After the photographs taken by the camera during the test were processed in MATLAB software, the displacement contour plots of different monitoring areas were derived, as shown in Figure 7, and displacement curves were obtained at different depths, as shown in Figure 8.

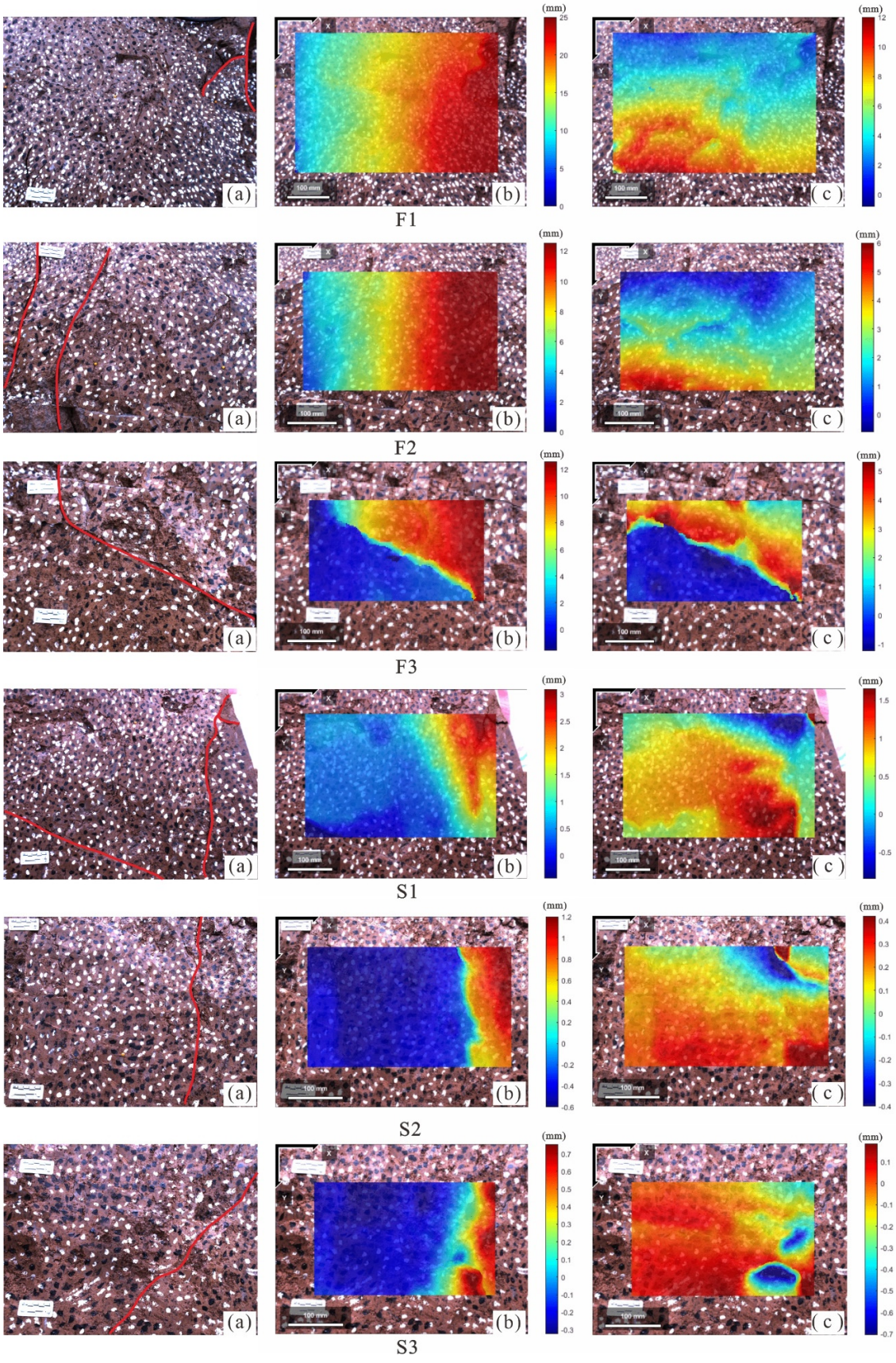

Figure 7. Slope displacement diagram: (**a**) final state of the slope (the red line indicates cracks that can be observed); (**b**) horizontal displacement obtained by the DIC method; and (**c**) vertical displacement obtained by the DIC method.

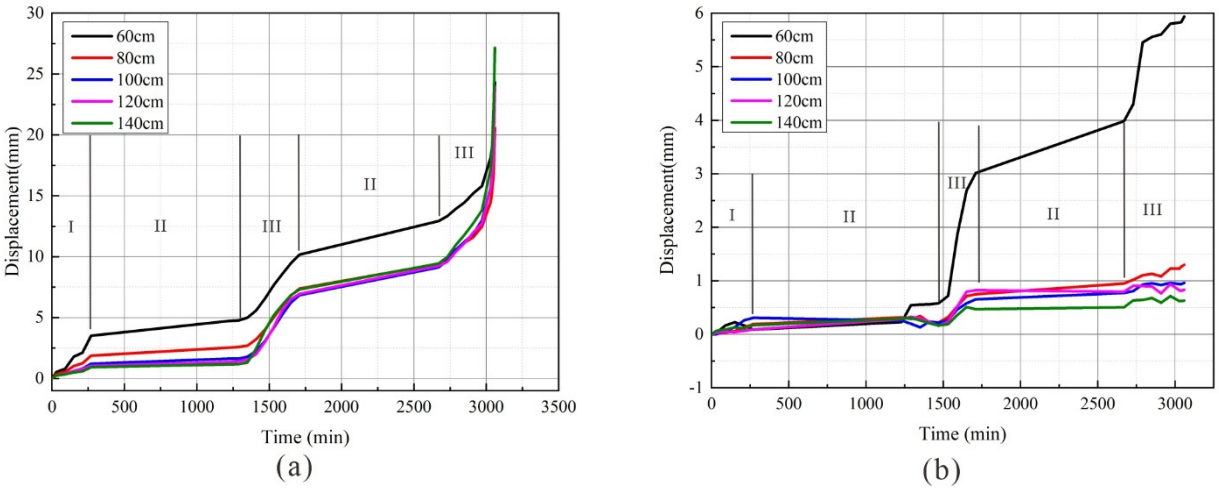

Figure 8. Displacement magnitudes of the slope at different depths (60 cm, 80 cm, 100 cm, 120 cm, 140 cm, corresponding to the vertical distance from the top of the slope): (**a**) displacement of the slope front; and (**b**) displacement of the slope side.

Figure 7 shows an obvious crack control effect in the deformation process of the expansive soil slope: the slope front (F1, F2 and F3) slid to the right along the horizontal direction, and the displacement was large on the right side. As determined from the vertical displacement results, F1 and F2 exhibited large displacements on the lower side of the slope, and the displacement on the upper right side of the crack in F3 was large, indicating that the soil at the slope front collapsed and slid to the right along the F3 crack. The displacement results of the slope side (S1, S2 and S3) show that the closer the slope was to the free face, the greater the displacement; furthermore, there was an obvious sliding effect along the crack, indicating that such cracks in the expansive soil destroyed the integrity of the soil. Meanwhile, rainwater infiltrated the soil along the cracks to accelerate slope instability and induce landslide disasters.

The average displacement–time curves derived at different depths (Figure 8) show that the deformation and failure of the expansive soil slope had an obvious "phased change law", and the displacement–time curve can be divided into three stages. The first stage was the slow deformation stage, the second stage was the stable deformation stage, and the third stage was the accelerated deformation stage. The slope of the deformation curve also increased rapidly until the whole slope was damaged. In addition, the closer to the top of the slope a given position was, the greater its horizontal displacement, while the farther from the top of the slope a given position was, the greater its vertical displacement. Figure 9 shows the average displacement–time curve of the monitored front and side areas of the studied slope. This displacement behaviour also reflected obvious phased characteristics. The slope had an obvious acceleration trend near 1500 min, and the displacement tended to stabilize at 1710 min. Some scholars have divided landslide types into steady-type landslides, exponential-type landslides, step-like landslides, and convergent-type landslides according to their unique displacement monitoring curves [28]. According to this classification, the landslide studied herein can be classified as a step-like landslide. In addition, the monitoring data show that the average displacement of the slope front before failure was greater than the average lateral displacement.

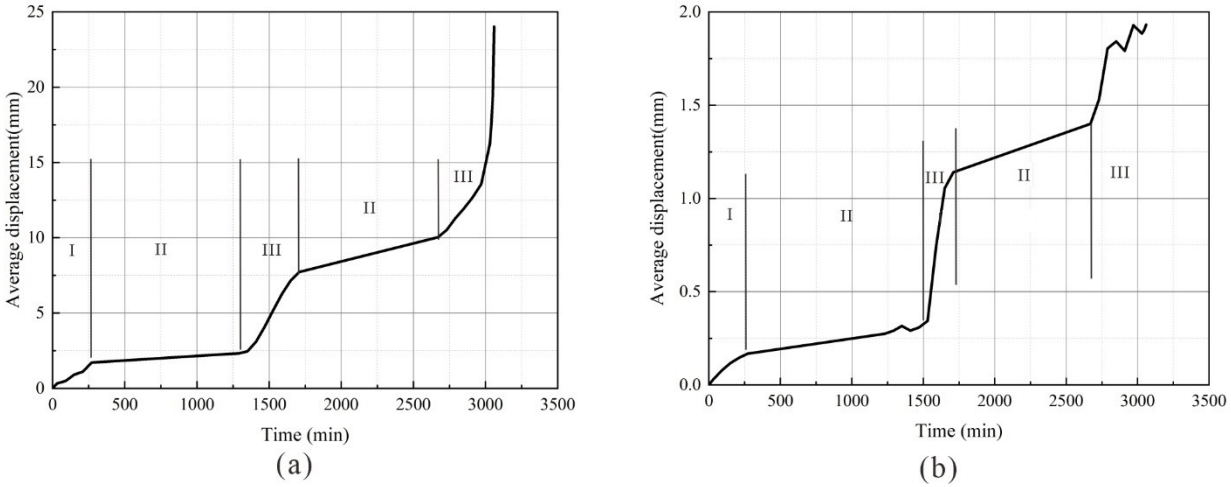

Figure 9. Average displacement magnitudes of the slope: (**a**) displacement of the slope front; and (**b**) displacement of the slope side.

The INV method was used to forecast the failure time of the slope. First, the average displacement monitoring data of the surface front and side of the slope were taken (Figure 9), and the average velocity at different monitoring time points was calculated to obtain the reciprocal time series points of the rate of displacement of different monitoring surfaces (Figure 10). The rate dispersion at different monitoring time points was large, and the $1/v$-t relationship curve is linear, so α was taken as 2. The fitting correlation coefficient of the reciprocal of the deformation rate of the slope R^2 are all less than 0.4, that means the model could not provide good prediction, the specific reasons will be discussed in detail below.

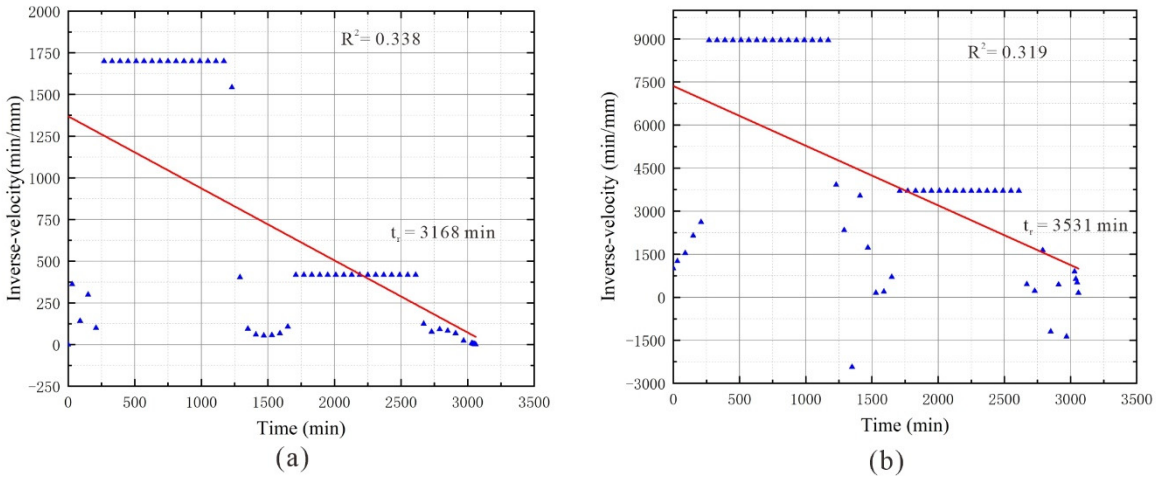

Figure 10. Typical plots used to predict slope failure using the INV method: (**a**) slope front; and (**b**) slope side.

The SLO method was used to forecast the failure time of the slope. First, the average displacement monitoring data of the front and side of the slope surface were determined (Figure 8), and the average velocity was calculated at different monitoring time points to obtain $t(du/dt)$-du/dt sequence points on different monitoring surfaces. As shown in Figure 11, there was an obvious linear discrete relationship between different monitoring time points, and the $t(du/dt)$-du/dt sequence points were fitted linearly. The fitting correlation coefficient of the reciprocal of the front deformation rate is $R^2 = 0.999$, and the front deformation monitoring test data are in good agreement with the fitting line. The coincidence degree between the lateral deformation monitoring test data and fitting line was relatively low, with $R^2 = 0.882$. According to these fitting results, the failure time of

the studied slope forecasted based on the SLO method using deformation data from the front of the slope was 3065 min, and the failure time predicted based on the deformation data from the side of the slope was 2697 min.

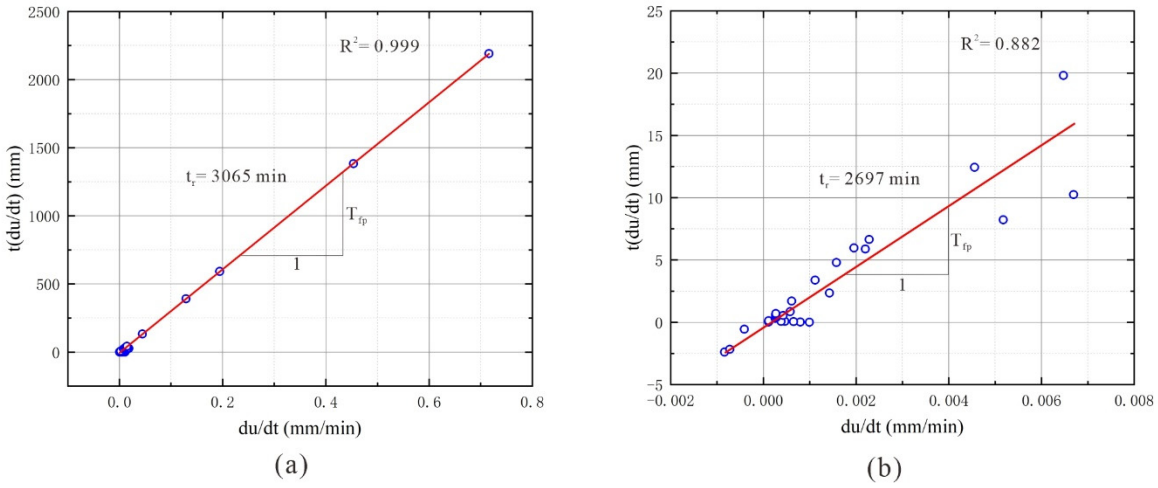

Figure 11. Typical plots used to predict slope failure using the SLO method: (**a**) slope front; and (**b**) slope side.

4. Discussion

The slope displacement–time curve shows that the displacement acceleration increased sharply when the slope deformation entered the failure stage before sliding. Taking the deformation rate of the slope as the early warning criterion to decide whether a landslide will occur is intuitive and reliable. Ref. [37] proposed a method to quantitatively describe the tangent angle of the landslide displacement–time curve and defined a new landslide failure threshold criterion based on this tangent angle. However, because the deformation rates of landslides are affected by many factors, such as the slope composition, deformation and failure modes, and external inducing factors, the deformation rates measured before the final instability can vary greatly, so it is difficult to obtain a certain threshold for obtaining accurate early warnings [27]. Therefore, the INV and SLO models were used to forecast the failure times of landslides in this paper.

The slope failure time recorded at the test site was 3060 min and compared with the prediction results of the INV method and SLO method, the forecast results of the SLO method were basically consistent with the actual failure time of the slope, indicating that the monitoring results of the DIC method can be used for landslide forecasting.

Expansive soil is characterized by strong fissures [38,39], and combined with the slope failure of the image monitoring results (Figure 12), it can be seen that the sliding of the slope results in obvious collapse only on the front and right sides. The failure at the left side of the slope is not obvious, leading to obvious errors in the resulting displacement monitoring curve characterizing the left side of the slope. The forecast results obtained with the INV method were obviously larger, while the prediction results derived through the SLO method were obviously smaller, suggesting that the accuracy of the forecast results was related to the selected monitoring location. The soft structure of the studied slope can control its stability; therefore, the displacement changes of the slope controlled by its structural plane should be the research focus. At the same time, limited by the photography technology itself, the DIC method can only measure the deformation of the shallow surface of the slope and cannot obtain the three-dimensional deformation inside the slope. However, compared with the DIC monitoring results of the deformation and failure of an indoor expansive soil slope model [36], it can be seen that this method has a good application for the acquisition of cracks in the shallow surface of expansive soil and that the field test displacement results of undisturbed soil are more discrete.

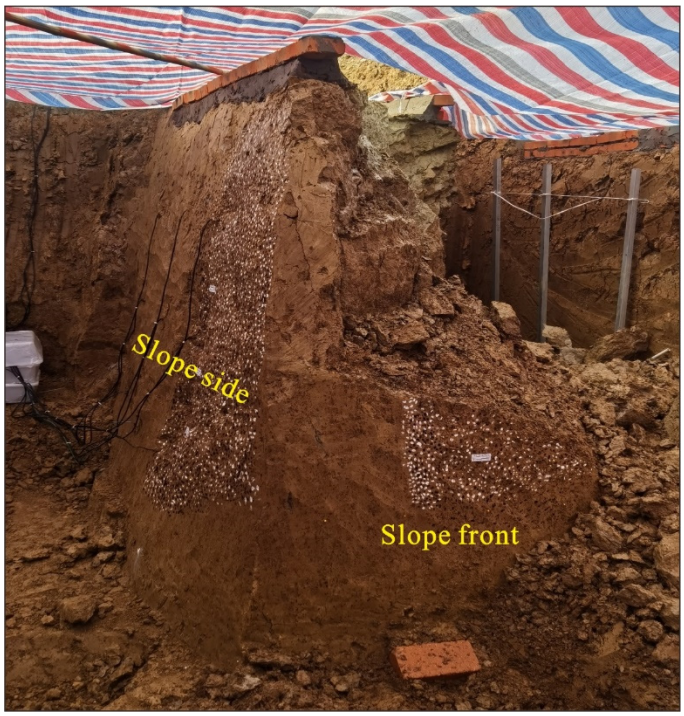

Figure 12. Shape of the slope after failure.

By comparing the forecast results obtained with the INV method and SLO method, due to the obvious control of the fissure structure of the expansive soil slope and the typical step-like landslide displacement curve, the calculation results of the INV method are more discrete, with higher linear fitting requirements, so the forecast results are too large. For the SLO method, the values obtained in the stable deformation stage are more concentrated in the calculation process, the method provides an obvious linear relationship only in the accelerated deformation stage, and the prediction results are thus more accurate. Therefore, the SLO method should be preferred for forecasting failures associated with step-like landslides.

Although the landslide monitoring technology and prediction method used in this paper can better forecast expansive soil landslides, theoretical modelling has not been verified due to three limitations. First, due to the limitations of the test site conditions, the excavated artificial slope is approximately vertical, unlike a natural slope. Second, because the DIC method can monitor the deformation rate of only the slope surface and the inducing factors of the deformation and failure of expansive soil are complex, it is impossible to directly predict the failure time of landslides through slope surface deformation results. Third, due to the limited number of tests, more field test data and monitoring results are needed for optimization and statistical analysis of the DIC method for landslide deformation monitoring and prediction. In the future, we will continue to focus on research related to deformation measurements based on the DIC method and forecasts of expansive soil landslides of this type to further optimize the proposed methodology and improve the accuracy of the calculated failure time [40].

5. Conclusions

In this study, a series of in situ artificial rainfall experiments were conducted on an excavated expansive soil slope. The DIC method was applied to monitor the slope surface deformation and crack development processes. Finally, the failure time of the slope was forecasted, and the results were discussed. The main conclusions are described as follows.

The DIC method can be effectively applied to the deformation measurement of expansive soil slopes, and the results show that there was an obvious crack control effect in the deformation process of the slope. The failure of the slope exhibited an obvious “phased

change law". The first stage was the slow deformation stage, the second stage was the stable deformation stage, and the third stage was the accelerated deformation stage. The slope of the deformation curve also increased rapidly until the whole slope was damaged.

According to the displacement–time curve results obtained by DIC, the INV method and SLO method were used to forecast the failure time of the slope. The results show that the data points calculated by the INV method were discrete and had high linear fitting requirements for expansive soil slopes, resulting in large, forecasted slope failure values. The SLO method was the most accurate method when applied to the slope front displacement monitoring data. Therefore, for expansive soil slopes with a step-like landslide displacement, the SLO method should be preferred over the INV method for failure forecasting.

Author Contributions: Conceptualization, W.G. (Wenwei Gao) and R.H.; methodology, X.W. and W.G. (Wenwei Gao); formal analysis, X.W. and W.G. (Wenwei Gao); writing—original draft preparation, X.W.; investigation, X.W., W.G. (Wei Gao), Y.Q. and Y.L.; writing—review and editing, X.W. and W.G.(Wenwei Gao); supervision, R.H.; project administration, R.H. and W.G. (Wei Gao); funding acquisition, R.H. All authors have read and agreed to the published version of the manuscript.

Funding: This research was funded by the National Key Research and Development Program of China, grant number 2019YFC1509902 and the National Natural Science Foundation of China, grant number 41977251.

Data Availability Statement: Data is contained within the article.

Acknowledgments: This work was supported by the National Key Research and Development Program of China (No. 2019YFC1509902) and the National Natural Science Foundation of China (No. 41977251). We greatly appreciate this financial support.

Conflicts of Interest: The authors declare no conflict of interest.

References

1. Ikeagwuani, C.C.; Nwonu, D.C. Emerging trends in expansive soil stabilisation: A review. *J. Rock Mech. Geotech. Eng.* **2019**, *11*, 423–440. [CrossRef]
2. Steinberg, M. Expansive soils and the geomembrane remedy. In *Advances in Unsaturated Geotechnics*; ASCE: Reston, VA, USA, 2000; pp. 456–466.
3. Bilir, M.E.; Sarıgül, G. Stability assessment of Terzili tunnel in swelling rock mass. *Arab. J. Geosci.* **2021**, *14*, 965. [CrossRef]
4. Leng, T.; Tang, C.; Xu, D.; Li, Y.; Zhang, Y.; Wang, K.; Shi, B. Advance on the engineering geological characteristics of expansive soil. *J. Eng. Geol.* **2018**, *26*, 112–128. [CrossRef]
5. Joshi, R.; Katti, R. Lateral pressure development under surcharges. In Proceedings of the Expansive Soils, Denver, CO, USA, 1 March 2011; pp. 227–241.
6. Lin, B.; Cerato, A.B. Prediction of expansive soil swelling based on four micro-scale properties. *Bull. Eng. Geol. Environ.* **2012**, *71*, 71–78. [CrossRef]
7. Preston, S.; Griffiths, B.; Young, I. An investigation into sources of soil crack heterogeneity using fractal geometry. *Eur. J. Soil Sci.* **1997**, *48*, 31–37. [CrossRef]
8. Vogel, H.-J.; Hoffmann, H.; Roth, K. Studies of crack dynamics in clay soil: I. Experimental methods, results, and morphological quantification. *Geoderma* **2005**, *125*, 203–211. [CrossRef]
9. Bao, C. Behavior of unsaturated soil and stability of expansive soil slope. *Chin. J. Geotech. Eng.* **2004**, *26*, 1–15.
10. Cheng, Y.; Cheng, Z.; Zhang, Y. Centrifugal model tests on expansive soil slope under rainfall. *Chin. J. Geotech. Eng.* **2011**, *33*, 409–414.
11. Kassiff, G.; Alpan, I. A Slope Failure in Swelling Clay. *Can. Geotech. J.* **1973**, *10*, 531–536. [CrossRef]
12. Zhan, L.-t.; Ng, W.-w.C.; Bao, C.-G.; Gong, B.-W. Artificial rainfall infiltration tests on a well-instrumented unsaturated expansive soil slope. *Rock Soil Mech.* **2003**, *24*, 151–158.
13. Dai, Z.; Chen, S.; Li, J. Physical model test of seepage and deformation characteristics of shallow expansive soil slope. *Bull. Eng. Geol. Environ.* **2020**, *79*, 4063–4078. [CrossRef]
14. Galeandro, A.; Doglioni, A.; Simeone, V.; Šimůnek, J. Analysis of infiltration processes into fractured and swelling soils as triggering factors of landslides. *Environ. Earth Sci.* **2014**, *71*, 2911–2923. [CrossRef]
15. George, A.M.; Chakraborty, S.; Das, J.T.; Pedarla, A.; Puppala, A.J. Understanding shallow slope failures on expansive soil embankments in north Texas using unsaturated soil property framework. In *PanAm Unsaturated Soils 2017*; ASCE: Reston, VA, USA, 2017; pp. 206–216. [CrossRef]

16. Khan, M.S.; Hossain, S.; Ahmed, A.; Faysal, M. Investigation of a shallow slope failure on expansive clay in Texas. *Eng. Geol.* **2017**, *219*, 118–129. [CrossRef]
17. Yang, Z.; Lv, J.; Shi, W.; Zhang, Q.; Lu, Z.; Zhang, Y.; Ling, X. Model Test Study on Stability Factors of Expansive Soil Slopes with Different Initial Slope Ratios under Freeze-Thaw Conditions. *Appl. Sci.* **2021**, *11*, 8480. [CrossRef]
18. Yang, Z.; Zhang, L.; Ling, X.; Li, G.; Tu, Z.; Shi, W. Experimental study on the dynamic behavior of expansive soil in slopes under freeze-thaw cycles. *Cold Reg. Sci. Technol.* **2019**, *163*, 27–33. [CrossRef]
19. Pei, P.; Zhao, Y.; Ni, P.; Mei, G. A protective measure for expansive soil slopes based on moisture content control. *Eng. Geol.* **2020**, *269*, 105527. [CrossRef]
20. Xie, C.; Ni, P.; Xu, M.; Mei, G.; Zhao, Y. Combined measure of geometry optimization and vegetation for expansive soil slopes. *Comput. Geotech.* **2020**, *123*, 103588. [CrossRef]
21. Reddy, P.S.; Mohanty, B.; Rao, B.H. Investigations for Chemical Parameters Effect on Swelling Characteristics of Expansive Soils. *KSCE J. Civ. Eng.* **2021**, *25*, 4088–4105. [CrossRef]
22. Toksöz Hozatlıoğlu, D.; Yılmaz, I. Shallow mixing and column performances of lime, fly ash and gypsum on the stabilization of swelling soils. *Eng. Geol.* **2021**, *280*, 105931. [CrossRef]
23. Zheng, S.; Yao, H.; Ge, X. Analysis of saturated and unsaturated seepage of cracked expansive soil. *Rock Soil Mech.* **2007**, *28*, 281–285. [CrossRef]
24. Kaiyu, R.; Xin, Y.; Xiaoming, Z.; Zhenkai, Z.; Lingjing, L. Study of landslide failure prediction based on TS-InSAR, GPS and image offset monitoring. *Chin. J. Rock Mech. Eng.* **2020**, *39*, 3421–3431. [CrossRef]
25. Saito, M. Forecasting time of slope failure by tertiary creep. In Proceedings of the 7th International Conference on Soil Mechanics and Foundation Engineering, Mexico City, Mexico, 1 January 1969; pp. 677–683.
26. Fukuzono, T. A method for predicting the failure time of a sandy soil slope using the inverse number of velocity. In Proceedings of the 23rd Meeting of Japan Landslide Society, Tokyo, Japan, 2 July 1984; pp. 80–81.
27. Mufundirwa, A.; Fujii, Y.; Kodama, J. A new practical method for prediction of geomechanical failure-time. *Int. J. Rock Mech. Min. Sci.* **2010**, *47*, 1079–1090. [CrossRef]
28. Miao, F.; Wu, Y.; Xie, Y.; Li, Y. Prediction of landslide displacement with step-like behavior based on multialgorithm optimization and a support vector regression model. *Landslides* **2018**, *15*, 475–488. [CrossRef]
29. Peters, W.; Ranson, W. Digital Imaging Techniques In Experimental Stress Analysis. *Opt. Eng.* **1982**, *21*, 213427. [CrossRef]
30. Feng, T.; Liu, X.; Scaioni, M.; Lin, X.; Li, R. Real-time landslide monitoring using close-range stereo image sequences analysis. In Proceedings of the 2012 International Conference on Systems and Informatics (ICSAI2012), Yantai, China, 19–20 May 2012; pp. 249–253.
31. Liu, W.-C.; Huang, W.-C. Close range digital photogrammetry applied to topography and landslide measurements. *ISPRS Int. Arch. Photogramm. Remote Sens. Spat. Inf. Sci.* **2016**, *XLI-B5*, 875–880. [CrossRef]
32. Travelletti, J.; Delacourt, C.; Allemand, P.; Malet, J.P.; Schmittbuhl, J.; Toussaint, R.; Bastard, M. Correlation of multi-temporal ground-based optical images for landslide monitoring: Application, potential and limitations. *ISPRS J. Photogramm. Remote Sens.* **2012**, *70*, 39–55. [CrossRef]
33. Sharafisafa, M.; Aliabadian, Z.; Shen, L. Crack initiation and failure development in bimrocks using digital image correlation under dynamic load. *Theor. Appl. Fract. Mech.* **2020**, *109*, 102688. [CrossRef]
34. Zhao, Y.; Wang, H.; Zhang, Q.; Xie, Y.; Yang, J. A study of landslide deformation field with digital correlation method. *Chin. Sci. Bull.* **2016**, *61*, 3163–3171. [CrossRef]
35. Fukuzono, T. A new method for predicting the failure time of a slope. In Proceedings of the 4th International Conference and Field Workshop on Landslide, Tokyo, Japan, 23–31 August 1985; pp. 145–150.
36. Jiming, Y.; Hongri, Z.; Lin, C.; Yongfu, X. Analysis of crack morphology evolution law of expansive soil slope based on digital image correlation technology. *J. Cent. South Univ.* **2022**, *53*, 225–238.
37. Xu, Q.; Yuan, Y.; Zeng, Y.; Hack, R. Some new pre-warning criteria for creep slope failure. *Sci. China Technol. Sci.* **2011**, *54*, 210–220. [CrossRef]
38. Baer, J.; Kent, T.; Anderson, S. Image analysis and fractal geometry to characterize soil desiccation cracks. *Geoderma* **2009**, *154*, 153–163. [CrossRef]
39. Peng, X.; Horn, R.; Peth, S.; Smucker, A. Quantification of soil shrinkage in 2D by digital image processing of soil surface. *Soil Tillage Res.* **2006**, *91*, 173–180. [CrossRef]
40. Chen, G.; Tang, P.; Huang, R.; Wang, D.; Lin, Z.; Huang, D. Critical tension crack depth in rockslides that conform to the three-section mechanism. *Landslides* **2021**, *18*, 79–88. [CrossRef]